Exploration of Zr doping in pulsed laser deposited α-Ga_2O_3 for device applications

S. Vogt,* C. Petersen, H. von Wenckstern,† and M. Grundmann
Universität Leipzig, Felix-Bloch-Institut für Festkörperphysik, 04103 Leipzig, Germany

T. Schultz and N. Koch
Humboldt Universität zu Berlin, Institut für Physik, Brook-Taylor-Straße 6, 12489 Berlin, Germany and Helmholtz-Zentrum Berlin für Materialien und Energie GmbH, 12489 Berlin, Germany

(Dated: May 6, 2024)

The feasibility of zirconium doping of α-Ga_2O_3 grown by pulsed laser deposition is demonstrated. Targets with different zirconium contents are used to adjust the zirconium content in the thin films. Therefore, a two-step growth process is utilized, where first an undoped α-Ga_2O_3 thin film is grown as high-temperature buffer layer and the zirconium doped α-Ga_2O_3 layer is subsequently deposited at a lower growth temperature. Highly conductive thin films are obtained with resistivities as low as 3.3×10^{-3} Ωcm. An electron mobility as high as $38\,cm^2V^{-1}s^{-1}$ is measured for a high free carrier density of $6.5 \times 10^{18}\,cm^{-3}$. The crystallization in the α-phase was confirmed by X-ray diffraction measurements. Further, a strong influence of the growth temperature on the zirconium incorporation is observed, which can be explained by the increased desorption of volatile Ga_2O_3 suboxides at high growth temperatures. Depth resolved x-ray photo-electron spectroscopy measurements were employed to investigate the doping profile in the thin films. They reveal a strongly depth dependent incorporation of the zirconium, with a decreased incorporation towards the surface. First Schottky barrier diodes on zirconium doped α-Ga_2O_3 thin films with rectification ratios as high as 8.5 orders of magnitude at ± 3 V are presented.

INTRODUCTION

With an ultra-wide band gap of up to 5.3 eV[1] the α-polymorph of gallium oxide is especially interesting for high power applications[2, 3] as well as transparent conductive thin films [4], and solar blind photo-detectors [2]. The corundum structured α-phase of Ga_2O_3 is not as well studied as the thermodynamically stable β-phase. However, due to a higher expected breakdown [5] field and first commercially available α-Ga_2O_3 based devices, the material has gained increased scientific interest. Numerous growth methods have been used to grow high-quality α-Ga_2O_3. Amongst them are mist chemical vapor deposition (CVD) [6–8], atomic layer deposition (ALD) [9], halide vapour phase epitaxy (HVPE) [10], molecular beam epitaxy (MBE) [11], sputtering [12], and pulsed laser deposition (PLD) [13–17]. The α-phase can be grown on readily available, cost-efficient and isostructural α-Al_2O_3 substrates. The materials current main drawback is the high dislocation density of up to $10^{10}\,cm^{-2}$ arising from the large lattice mismatch with the substrate and the different thermal expansion coefficients of Al_2O_3 and Ga_2O_3 [18, 19]. This severely limits the electron mobility in α-Ga_2O_3 thin films. The dislocation density can be reduced by the use of binary α-Ga_2O_3 as well as by vertically graded $(Al_xGa_{1-x})_2O_3$ buffer layers [20–23]. Therewith, the edge dislocation density could be significantly reduced to about $10^8\,cm^{-2}$. A low dislocation density is crucial, as threading dislocations act – similarly to what is observed for GaN - as scattering centers [24]. Utilizing buffer layers, electron mobilities as high as $37\,cm^2V^{-1}s^{-1}$ at a free carrier concentration of $3.7 \times 10^{18}\,cm^{-3}$ for germanium doping [16], $51\,cm^2V^{-1}s^{-1}$ at a free carrier concentration of $2 \times 10^{18}\,cm^{-3}$ for silicon doping [25] and $65\,cm^2V^{-1}s^{-1}$ at a free carrier concentration of $1 \times 10^{18}\,cm^{-3}$ for tin doping [21] have been achieved. This is, however still far below the theoretically calculated electron mobility of α-Ga_2O_3 thin films, which is expected to exceed the $250\,cm^2V^{-1}s^{-1}$ for β-Ga_2O_3 [3]. Therefore, the need for further optimization of buffer layers and the exploration of different dopants arises. A promising shallow donor in β-Ga_2O_3 is zirconium [26–28]. Therewith, electron mobilities as high as $112\,cm^2V^{-1}s^{-1}$ could be achieved in single crystals at room temperature and the activation energy was determined as ≈ 10 meV[28]. Furthermore, theoretical calculations by Wickramaratne *et al.* predict that zirconium remains a shallow donor in the α-$(Al_xGa_{1-x})_2O_3$ alloy up to aluminum contents of $x \approx 0.38$[29]. This exceeds the calculated limits of tin ($x \approx 0.32$) and germanium ($x \approx 0.06$), which renders zirconium an interesting dopant for α-Ga_2O_3 and the α-$(Al_xGa_{1-x})_2O_3$ alloy [29].

In this work, the feasibility of α-Ga_2O_3 doping by zirconium on m-plane sapphire substrates is investigated for the first time to the best knowledge of the authors. The influence of the offered zirconium content as well as of the growth temperature on the electrical and structural properties is analyzed. X-ray photo-electron spectroscopy measurements are used to determine the zirconium incorporation in dependence on the growth temperature for two different zirconium contents in the target. Properties of first Schottky barrier diodes based on α-Ga_2O_3:Zr are presented and discussed for two different zirconium contents.

EXPERIMENTAL METHOD

All thin films were grown by pulsed laser deposition on $10 \times 10\,mm^2$ single side polished m-plane (10.0) sapphire by CrysTec with a miscut $< 0.1°$. The ablation was performed with a KrF excimer laser ($\lambda = 248$ nm). A pulse frequency of 20 Hz was used. The targets were fabricated from gallium oxide powder (purity 99.999% by Alfa Aesar) mixed with varying zirconium oxide (purity 99.978% by Alfa Aesar) of 1 wt.%, 0.5 wt.%, 0.025 wt.%, or 0.001 wt.% for the individual targets. Therefore, the powders were mixed and ground in a ball mill. Subsequently, a cylindrical target was pressed and sintered at 1300°C for 72 h in ambient atmosphere. For all thin films, a two step approach was used, as previously described [16]. The binary α-Ga_2O_3 buffer was deposited with 10k pulses at 580°C[17], whereas the α-Ga_2O_3:Zr layer was deposited with 15k pulses. All thin films were deposited in a 3×10^{-4} mbar O_2 atmosphere. The buffer layer thickness is 80 nm for all thin films. The thickness of the active layer depends on the growth temperature and was determined as 450 nm for a growth temperature $T_g = 465°C$ and 250 nm for $T_g = 540°C$. A decreasing layer thickness for higher growth temperatures is expected due to the desorption of volatile gallium sub-oxides[17].

The thickness of the thin films was determined by spectroscopic ellipsometry using a RC2, J.A. Woollam M2000. X-ray diffraction (XRD) measurements were employed to investigate the crystallographic structure using an Philips X'Pert diffractometer. The XPS measurements were performed at the Humboldt Universität zu Berlin with a JEOL JPS-9030 setup, using a non-monochromated aluminum source for excitation. A hemispherical analyzer with a pass energy of 30 eV was used for detection of the photoelectrons. No charge compensation was employed. The binding energy scale was calibrated by measuring sputter cleaned gold and copper reference samples and setting the Au4$f_{7/2}$ peak to 84.0 eV and the Cu2$p_{3/2}$ peak to 932.6 eV. Argon was used as sputter gas ($p_{Ar} = 3 \times 10^{-4}$ mbar) for depth profiling. A low acceleration voltage of 300 V and an ion current of 3.5 mA were used to avoid sputter damage. The sensitivity factors were determined by measuring pure Ga_2O_3 and ZrO_2 reference samples and assuming perfect stoichometry.

For the electrical characterization, Ti/Al/Au contacts with a thickness of 30 nm/30 nm/30 nm were thermally evaporated on the sample corners. An annealing in nitrogen atmosphere at a temperature of 410°C for 20 minutes was used to enable ohmic behavior of the contacts [30]. All thin films were characterized electrically by direct current Hall-effect and resistivity measurements in van der Pauw geometry using a home-built set-up [31–33]. The ohmic contacts on the thin film corners were small (3-4 mm^2 per contact) compared to the sample size (100 mm^2). The resistivity and Hall-effect measurements were performed in the dark using a magnetic field of 0.43 T. Current - voltage characteristics were recorded by employing a Süss Waferprober System P200 connected to an Agilent 4155C Semiconductor Parameter Analyzer. The lateral Schottky barrier diodes were realized by reactively sputtered platinum in a 50/50 O_2/Ar atmosphere, capped with a metallic platinum layer [34].

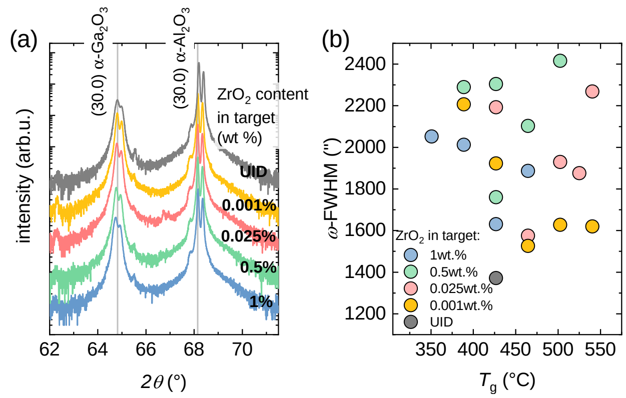

FIG. 1. X-ray diffractogram (a) for different zirconium oxide contents in the target material with a distinct (30.0) α-Ga_2O_3 reflex and (b) full width at half maximum (FWHM) determined from rocking curves in dependence on the growth temperature T_g. Outside the shown 2θ-range, no further peaks were observed.

EXPERIMENTAL RESULTS

In β-Ga_2O_3, zirconium has been reported to be a shallow donor, similar to silicon or tin. However, up to now no experiments exist on zirconium doped α-Ga_2O_3. Calculations by Wickramaratne *et al.* [29] also predict low formation energy for the incorporation of Zr^{4+} on the Ga site. Targets with four different zirconium contents were fabricated, namely 1 wt.%, 0.5 wt.%, 0.025 wt.%, and 0.001 wt.%. The α-phase could be stabilized for all four zirconium contents, as is exemplary shown for a growth temperature $T_g = 465°C$ in Figure 1(a). In the X-ray diffractograms a distinct (30.0) reflex is visible for all zirconium contents and no additional reflexes were observed outside the range shown. The crystal mosaicity of the thin films was determined by the full width at half maximum (FWHM) obtained from ω rocking curves (compare Figure 1(b)). Since relaxed α-Ga_2O_3 grows with an inclined c-axis on m-plane sapphire[35], all samples were azimuthally aligned with the c-plane parallel to the inciendent beam to allow for comparable results of the rocking curves. For all dopant concentrations, an expected increase of the FWHM to lower growth temperatures is observed, which has also been observed for undoped α-Ga_2O_3 thin films [17]. For growth temperatures of $425°C < T_g < 500°C$, a decrease of FWHM is observed. For growth temperatures above 450°C, the thin films which were grown from the 0.001 wt.% ZrO_2 doped target exhibit, as expected, the lowest FWHM values, with a minimum value of 1526" obtained for $T_g = 465$ °C. This is most likely due to less distortions in the lattice with less dopant offered, as zirconium has a significantly larger atomic and ionic radius than gallium. The atomic radii of zirconium and gallium are 155 pm and 130 pm, respectively [36], while the ionic radii of Ga^{3+} and Zr^{4+} are 76 pm and 86 pm [37]. With higher growth temperatures, a further improvement of the crystal quality was expected, which can not be observed. Akaiwa *et al.* reported that tin doping improves the crys-

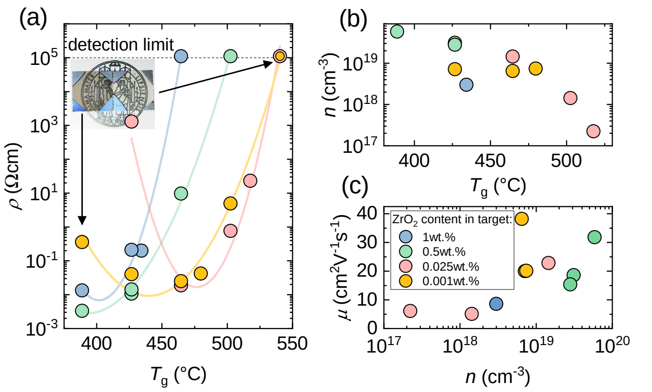

FIG. 2. Resistivity (a) and carrier concentration (b) in dependence on the growth temperature T_g for different zirconium oxide contents in the target. In (a) a photographic image of a thin film grown from a 0.001 wt.% ZrO_2 doped target deposited at 390°C and 540°C is shown. In (c) the electron mobility is shown in dependence on the free carrier density for the different offered dopant concentrations during growth.

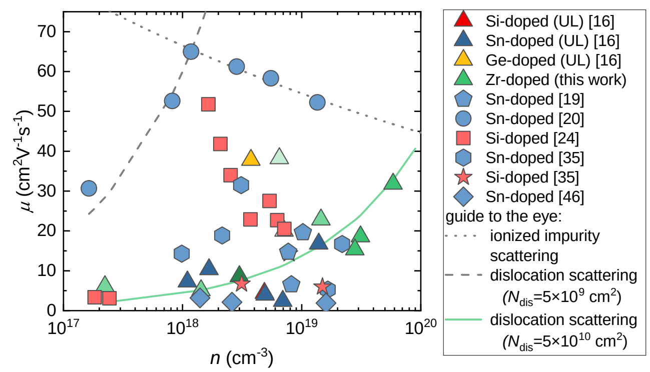

FIG. 3. Electron mobility versus free carrier density of results obtained in this work and published in literature. For high carrier concentrations, it is assumed that the electron mobility is limited by ionized impurity scattering (guide to the eye indicated by dotted line), whereas for small carrier concentrations, it is limited by scattering on dislocations (guide to eye indicated by dashed line and green line). The zirconium concentration in the target is indicated by darker green (1 wt.%) to lighter green (for less zirconium). References for the data given in the legend. UL denotes University Leipzig.

tal quality compared to unintentionally doped α-Ga_2O_3 thin films [20]. This effect can not be observed for zirconium doping, which again is likely due to the larger atomic radius.

In electrical measurements, a strong dependence of the resistivity on the zirconium content in the target as well as on the growth temperature is observed. For ZrO_2 contents in the target of 1 wt.% and 0.5 wt.%, a minimum resistivity is observed for the lowest growth temperature of 390°C (compare Figure 2(a)). A minimum value as low as 3.3×10^{-3} Ωcm is measured for 0.5 wt.% ZrO_2 in the target. For 0.025 wt.% ZrO_2 and 0.001 wt.% ZrO_2 in the targets, a very similar minimum value of the resistivity is observed at 465°C. For low growth temperatures, the resistivity most likely increases due to the decreased crystal quality as observed in the rocking curves. This can also be seen in the brownish color of the thin film shown in the inset in Figure 2(a), which is an indication of a high number of defects and/or oxygen deficiency. The onset T_g for that brownish color strongly depends on the dopant content offered in the target. For 1 wt.% ZrO_2 in the target, even the thin film grown at $T_g = 390$°C is still transparent, whereas thin films deposited at this temperature for smaller zirconium contents in the target already turn brownish. For high growth temperatures, a strong increase of the resistivity is observed for all dopant concentrations. The loss of conductivity for high growth temperatures has been observed before for tin, silicon and germanium doping and was attributed either to an evaporation of the dopant or due to a change in charge state, such that the dopant no longer contributed to the electrical conductivity [16, 38]. For a temperature of 465°C, a tuning of the resistivity from 1.8×10^{-2} Ωcm to 9.6 Ωcm can be achieved by increasing the offered amount of dopant from 0.001 wt.% to 0.5 wt.%.

Hall-effect measurements were performed on all thin films to obtain the free carrier density and the electron mobility. A decrease of the free carrier density over two orders of magnitude with increasing growth temperature is observed for a zirconium content of 0.025 wt.% in the target (compare Figure 2(b)). For all other zirconium concentrations, too few measurement values were obtained to observe a dependence on the growth temperature. Furthermore, the highest carrier density of 5.8×10^{19} cm^{-3} is obtained for 0.5 wt.% ZrO_2 in the target, which is even higher than the carrier density we obtained for tin doped thin films [16]. The electron mobility, shown in Figure 2(c), does not exhibit a dependence on the growth temperature. It does however, show a dependence on the free carrier density. With increasing carrier concentration the electron mobility also increases. The highest electron mobility of 38 cm^{2}V^{-1}s^{-1} is observed for the thin film with the smallest FWHM$_\omega$.

This is the – up to now – highest achieved electron mobility at such a high carrier density for doped α-Ga_2O_3, as can be seen in Figure 3, which depicts the electron mobility in dependence on the free carrier density for different dopants compiling various results from literature. Here also the exceptionally high electron mobility for carrier densities above 10^{19} cm^{-3} is immediately visible. Assuming, that the decrease of the mobility for high carrier density is solely due to ion impurity scattering, the mobility depends on the free carrier density as [39, 40]

$$\mu_{\text{ion}} \propto \frac{1}{N_{\text{ion}}} , \tag{1}$$

Where the density of ionized donors N_{ion} was approximated by the free carrier density n. This was done to calculate a guide to the eye how the electron mobility decreases for increasing carrier density, which is shown as gray, dotted line.

On the other hand for small carrier densities, the mobility mainly decreases due to scattering on dislocation lines in crys-

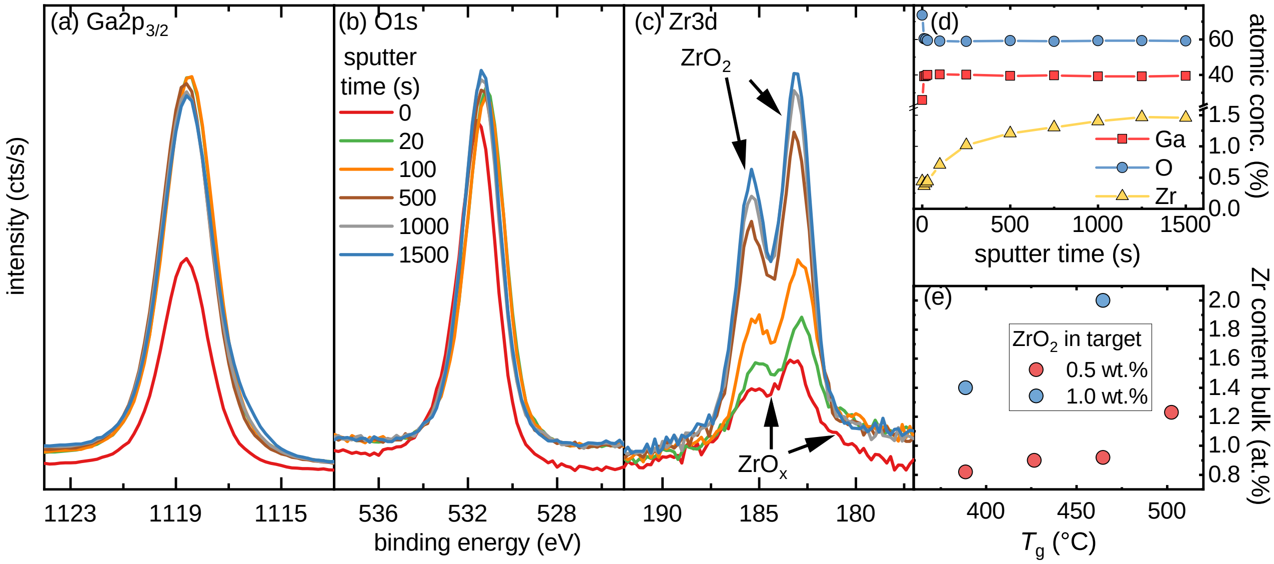

FIG. 4. Signal intensity in dependence on the binding energy for (a) $Ga2p_{3/2}$, (b) O1s and (c) Zr3d for different sputtering times. The extracted atomic concentrations as a function of the sputter time are depicted in (d) for one exemplary sample grown at $T_g = 500°C$ from the target containing 1wt.% ZrO_2. Bulk zirconium content for different growth temperatures and two different ZrO_2 concentrations in the target (e).

talline α-Ga_2O_3. This can be approximated by [41, 42]:

$$\mu_{dis} \propto \frac{\sqrt{n}}{N_{dis}} T \ . \tag{2}$$

A dislocation density of approximately $5 \times 10^9\ cm^{-2}$ was obtained for a fit on the data by Akaiwa *et al.* in the low carrier concentration range [21]. This is shown by the gray, dashed line as guide to the eyes in Figure 3. If one uses the same approach to fit the electron mobilities obtained on zirconium doped α-Ga_2O_3, a dislocation density as high as $5 \times 10^{10}\ cm^{-2}$ has to be assumed to approximate the correlation between electron mobility and free carrier density. This is shown as green, solid line in Figure 3. However, this is only a rough estimate, as other measurement techniques, such as transmission electron microscopy, would be required to measure the dislocation density of the zirconium doped thin films. Furthermore, this approximation neglects the simultaneous influence of ionized impurity scattering, which commonly is the limiting factor for the electron mobility for these high carrier densities.

To gain a more profound understanding of the zirconium incorporation into the thin films, X-ray photo-electron spectroscopy measurements were performed. The depth dependent measurements were performed for different growth temperatures and for 1 wt.% and 0.5 wt.% ZrO_2 in the target. For lower zirconium contents in the target, measurements were not feasible due to the elemental detection limit of the XPS method. In Figure 4(a-c) the intensity of the $Ga2p_{3/2}$, O1s and Zr3d peak for different sputter times are depicted. For zirconium, predominantly ZrO_2 and some additional signal from ZrO_x is measured at the surface (see Figure 4(c)), whereas only ZrO_2 is detected in the bulk (i.e. for sputter times above 100 s). Furthermore, the zirconium content is strongly depth dependent, as is shown in Figure 4(d) for $T_g = 390°C$ and 1wt.% ZrO_2 in the target. At the surface a zirconium content of 0.5 at.% is measured, which increases to a value of 1.5 at.% in the bulk thin film. This increase occurred over a sputtering time of approximately 1200 s, which corresponds to a sputtering depth of about 200 nm. This corresponds to a very inhomogeneous depth dependent incorporation of the zirconium. This also has to be taken into account when interpreting the Hall-effect measurements, as the resistivity is likely overestimated whereas the free carrier density is underestimated due to the in-homogeneity. The electron mobility is not influenced by a different active layer thickness, as expected from the inhomogeneous donor profile.

To understand whether this effect is due to an evaporation of zirconium from the thin film during the cool down of the thin film or occurs already during the growth, a sample with an in-situ, 20-30 nm thick Al_2O_3 capping was grown at the same growth temperature of $T_g = 465°C$ as the doped layer.

Depth resolved XPS measurements were performed on this sample, which disclose a homogeneous/reduced gradient of the zirconium incorporation (see Figure S2 for a detailed XPS analysis [43]). This is a strong indication that zirconium evaporates from the thin film during the cool down phase after the deposition. Further investigations have to show whether this doping gradient can be prevented if the cool down occurs in oxygen ambient with 800 mbar rather than at 3×10^{-4} mbar.

An increase of the zirconium incorporation with increasing growth temperature is observed, which might explain the reduced crystal quality for higher growth temperatures and

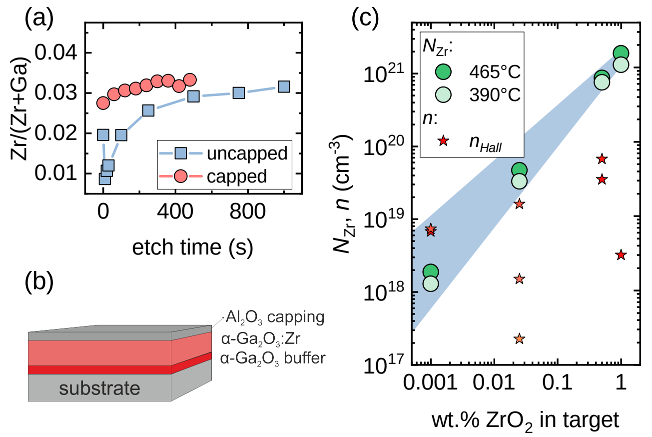

FIG. 5. In (a) the depth resolved zirconium content determined by XPS for an uncapped and an Al_2O_3 capped film deposited from a target consisting of 0.5 wt.% ZrO_2 at 500°C and in (b) the schematic layout for the capped thin film. (c) Number of zirconium atoms N_{Zr} per cubic centimeter and free carrier density in dependence on the zirconium oxide content in the target. For zirconium oxide contents $\leq$ 0.025 wt.%, the number of zirconium atoms is estimated from the transfer rate for the thin films deposited from the targets with ZrO_2 contents $\geq$ 0.5 wt.% and an approximated error margin is given in blue.

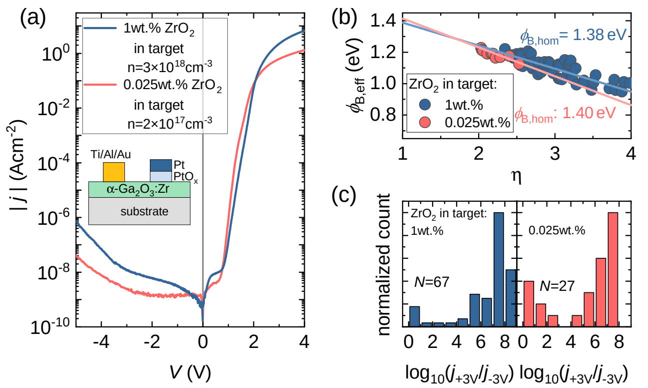

FIG. 6. (a) Current density (j)-voltage (V) characteristics for the diodes with the highest rectification ratio on two thin films fabricated from different targets as denoted. In (b) the effective barrier height $\phi_{B,\mathrm{eff}}$ is depicted as function of the ideality factor η and in (c) statistics of the logarithm to base 10 of the rectification ratio of all devices on these two thin films are depicted. The total number of diodes N is denoted in (c).

the high resistivity of these thin films. For 1 wt.% ZrO_2 in the target, the zirconium content at high growth temperatures of $T_g = 465$°C is at Zr/(Zr+Ga)=0.05. This is alloying rather than doping. The increase of the zirconium content in the thin films with increasing growth temperature is likely due to the desorption of gallium suboxides during the growth, which is more pronounced for higher growth temperatures. In contrast, for tin doping of α-Ga_2O_3 a lower tin incorporation with increasing growth temperature was observed [16]. Furthermore, the transfer of zirconium from the target into the thin film at a given growth temperature is directly proportional to the amount of zirconium in the target.

Using the thus obtained zirconium contents in the thin films, the number of zirconium atoms per cubic centimeter N_{Zr} was calculated for ZrO_2 contents in the target of 1 wt.% and 0.5 wt.%. These results and an assumption of a similar transfer for lower zirconium contents in the target were used to estimate N_{Zr} for ZrO_2 contents in the target of 0.025 wt.% and 0.001 wt.%. This is depicted in Figure 5(c) with a wide error range for smaller zirconium contents. In addition, the free carrier densities determined for these dopant concentrations (for all growth temperatures) are depicted as well. Assuming the same transfer rate of zirconium for 0.001 wt.% ZrO_2 in the target as for the higher contents, the free carrier density would be higher than the amount of N_{Zr}. We can exclude that unintentional doping is causing this high carrier density, as nominally undoped α-Ga_2O_3 thin films deposited at the same conditions do not exhibit any conductivity. We therefore conclude that the zirconium transfer must be higher than expected from our estimations. For high zirconium contents in the target, there are one to two order of magnitude more zirconium atoms in the thin film than free carriers. It is yet unclear whether these zirconium atoms are evenly distributed in the thin film or whether a clustering or accumulation on dislocation lines occurs. The doping efficiency was estimated by first calculating the total number of zirconium atoms per unit volume and then relating this to the free carrier density. A maximal doping efficiency of 2% and 8% were obtained for 1 wt.% and 0.5 wt.% ZrO_2 in the target, respectively. For lower zirconium contents in the target the value can not be calculated, as the zirconium contents in the thin film are only approximated. However, we assume that the doping efficiency further increases with decreasing zirconium content in the target.

Using two thin films with carrier densities of 3×10^{18} cm^{-3} ($T_g = 435$°C, 1 wt.% ZrO_2 in target) and 2×10^{17} cm^{-3} ($T_g = 520$°C, 0.025 wt.% ZrO_2 in target), lateral Schottky barrier diodes were fabricated. The obtained current density (j) – voltage (V) characteristics are depicted in Figure 6(a). A high forward current density of 2.0 Acm^{-2} and 0.6 Acm^{-2} is measured at +3 V for the diodes on thin films deposited from the 1 wt.% ZrO_2 and 0.025 wt.% ZrO_2, respectively. The higher forward current for the diode from the 1 wt.% ZrO_2 target is expected from the higher carrier density resulting in a lower series resistance. In the reverse regime, a lower current density is observed for the diodes on the thin film deposited from the 0.025 wt.% ZrO_2 target for $V \leq -3$ V. The higher forward current as well as the higher reverse current are expected for higher carrier densities in the thin film. At $V = -2$ V, the onset of a increase of the current is measured for the diode from the 0.025 wt.% ZrO_2. From the exponential increase, a tunneling current is probable, however temperature dependent $j-V$ measurements are required to confirm this. For both thin films, a $j-V$ characteristic of the contact with the highest rectification ratio is shown for a voltage sweep from

0 V to −5 V and from 0 V to +4 V. In forward direction, the additional influence of a charging current is observed, which can also be seen for a voltage sweep from negative to positive voltage and vice versa (compare Figure SI2, which depicts the current-voltage characteristics for both voltage sweep directions [43]) [44, 45]. Assuming thermionic emission to be the dominant transport mechanism, the effective barrier height $\phi_{\mathrm{B,eff}}$ was obtained from the current-voltage characteristics in negative voltage sweep direction. It is depicted in Figure 6(b) as a function of the ideality factor η. By a linear fit, the homogeneous barrier height $\phi_{\mathrm{B,hom}}$ was extracted. Homogeneous barrier heights of $\phi_{\mathrm{B,hom}} \approx 1.4$ eV were obtained for both thin films. This is very similar for both thin films and comparable to similarly fabricated Schottky barrier diodes on tin doped α-Ga_2O_3 [34]. Overall, the ideality factor, with a lowest value of $\eta = 2$, is very high compared to Schottky barrier diodes on β-Ga_2O_3 [46]. The series resistance of the two diodes shown in Figure6(a) is $9.3 \times 10^6\,\Omega$ and $5.5 \times 10^7\,\Omega$ for 1 wt.% and 0.025 wt.% in the target, respectively. This corresponds well to the obtained resistivities of the samples. The rectification ratio S_{V}, calculated as the current at +3 V divided by the current at −3 V, is as high as 8.5 orders of magnitude. However, a strong variance in device performance is observed in the distribution of the rectification ratio in Figure 6(c). The rectification ratio of all contacts on the respective thin films are depicted, thus including contacts with shunts and/or ohmic behaviour. The large variance is due to either interface defects introduced during the sputtering or it might be due to the high zirconium concentration in the thin film, which leads to an increased tunneling probability. Further investigations are required to exclude a clustering of zirconium in the thin films. In addition, optimization steps of the thin film growth as well as for the Schottky barrier metal composition are required to improve the diode performance.

CONCLUSION

In summary, we have demonstrated the feasibility of zirconium doping in phase pure α-Ga_2O_3 for four different ZrO_2 contents in the target material and for different growth temperatures. Highly conductive thin films with a resistivity as low as $3 \times 10^{-3}\,\Omega$cm were obtained. Electron mobilities as high as $38\,\mathrm{cm^2V^{-1}s^{-1}}$ at a free carrier density of $6.5 \times 10^{18}\,\mathrm{cm^{-3}}$ were measured. This is the highest electron mobility reported for α-Ga_2O_3 thin films at such high carrier densities and demonstrates the great potential of zirconium doping of α-Ga_2O_3. An inhomogeneous depth dependent zirconium incorporation was detected by depth resolved XPS measurements. Thereby, less zirconium is incorporated at the surface, compared to the bulk thin film. The transfer of zirconium into the thin film strongly depends on the growth temperature, which is likely due to the high rate of gallium suboxides desorption during growths. As this effect is strongly temperature dependent, a higher desorption of gallium suboxides - and therewith a higher Zr content in the thin films - is observed for higher growth temperatures. First α-Ga_2O_3:Zr based diodes were presented which have high current rectification ratios of 8.5 orders of magnitude and homogeneous barrier height of 1.4 eV at room temperature.

We acknowledge the support of M. Hahn for target and contact fabrication. C.P. is supported by Build Mona and S.V. by Ultraspec. This work was partially performed in the framework of GraFOx, a Leibniz-Science Campus partially funded by the Leibniz Association.

DATA AVAILABILITY STATEMENT

The data that support the findings of this study are available from the corresponding author upon reasonable request.

* sofie.vogt@physik.uni-leipzig.
† wenckst@physik.uni-leipzig.de.

[1] A. Hassa, M. Grundmann, and H. von Wenckstern, Progression of group-III sesquioxides: epitaxy, solubility and desorption, Journal of Physics D: Applied Physics **54**, 223001 (2021).

[2] J. Zhang, J. Shi, D.-C. Qi, L. Chen, and K. H. L. Zhang, Recent progress on the electronic structure, defect, and doping properties of Ga_2O_3, APL Materials **8**, 020906 (2020).

[3] M. Higashiwaki, K. Sasaki, H. Murakami, Y. Kumagai, A. Koukitu, A. Kuramata, T. Masui, and S. Yamakoshi, Recent progress in Ga_2O_3 power devices, Semiconductor Science and Technology **31**, 034001 (2016).

[4] N. Suzuki, S. Ohira, M. Tanaka, T. Sugawara, K. Nakajima, and T. Shishido, Fabrication and characterization of transparent conductive Sn-doped β-Ga_2O_3 single crystal, physica status solidi (c) **4**, 2310 (2007).

[5] M. Biswas and H. Nishinaka, Thermodynamically metastable α-, ε- (or κ-), and γ-Ga_2O_3: From material growth to device applications, APL Materials **10**, 060701 (2022).

[6] S. Fujita and K. Kaneko, Epitaxial growth of corundum-structured wide band gap III-oxide semiconductor thin films, Journal of Crystal Growth **401**, 588 (2014).

[7] K. Kaneko, K. Suzuki, Y. Ito, and S. Fujita, Growth characteristics of corundum-structured α-$(Al_x\,Ga_{1-x})_2O_3$/Ga_2O_3 heterostructures on sapphire substrates, Journal of Crystal Growth **436**, 150 (2016).

[8] G. T. Dang, T. Yasuoka, Y. Tagashira, T. Tadokoro, W. Theiss, and T. Kawaharamura, Bandgap engineering of α-$(Al_xGa_{1-x})_2O_3$ by a mist chemical vapor deposition two-chamber system and verification of Vegard's Law, Applied Physics Letters **113**, 062102 (2018).

[9] J. Roberts, J. Jarman, D. Johnstone, P. Midgley, P. Chalker, R. Oliver, and F.-P. Massabuau, α-Ga_2O_3 grown by low temperature atomic layer deposition on sapphire, Journal of Crystal Growth **487**, 23 (2018).

[10] V. I. Nikolaev, A. I. Pechnikov, V. V. Nikolaev, M. P. Scheglov, A. V. Chikiryaka, S. I. Stepanov, O. S. Medvedev, S. V. Shapenkov, E. V. Ubyivovk, and O. F. Vyvenko, HVPE growth of α- and ε-Ga_2O_3 on patterned sapphire substrates, Journal of Physics: Conference Series **1400**, 055049 (2019).

[11] R. Kumaran, T. Tiedje, S. E. Webster, S. Penson, and W. Li, Epitaxial Nd-doped α-$(Al_{1-x}Ga_x)_2O_3$ films on sapphire for

solid-state waveguide lasers, Optics Letters **35**, 3793 (2010).

[12] M. Zubkins, V. Vibornijs, E. Strods, E. Butanovs, L. Bikse, M. Ottosson, A. Hallén, J. Gabrusenoks, J. Purans, and A. Azens, Deposition of Ga_2O_3 thin films by liquid metal target sputtering, Vacuum **209**, 111789 (2023).

[13] M. Lorenz, S. Hohenberger, E. Rose, and M. Grundmann, Atomically stepped, pseudomorphic, corundum-phase α-$(Al_{1-x}Ga_x)_2O_3$ thin films ($0 \leq x < 0.08$) grown on R-plane sapphire, Applied Physics Letters **113**, 231902 (2018).

[14] M. Grundmann and M. Lorenz, Anisotropic strain relaxation through prismatic and basal slip in α-(Al, Ga)$_2$O$_3$ on R-plane Al_2O_3, APL Materials **8**, 021108 (2020).

[15] A. Hassa, P. Storm, M. Kneiß, D. Splith, H. von Wenckstern, M. Lorenz, and M. Grundmann, Structural and Elastic Properties of α-$(Al_xGa_{1-x})_2O_3$ Thin Films on (11.0) Al_2O_3 Substrates for the Entire Composition Range, physica status solidi (b) **258**, 2000394 (2021).

[16] S. Vogt, C. Petersen, M. Kneiß, D. Splith, T. Schultz, H. von Wenckstern, N. Koch, and M. Grundmann, Realization of Conductive n-Type Doped α-Ga_2O_3 on m-Plane Sapphire Grown by a Two-Step Pulsed Laser Deposition Process, Physica Status Solidi (A) Applications and Materials Science **220**, 2 (2023).

[17] C. Petersen, S. Vogt, M. Kneiß, H. von Wenckstern, and M. Grundmann, PLD of α-Ga_2O_3 on m-plane Al_2O_3: Growth regime, growth process, and structural properties, APL Materials **11**, 1 (2023).

[18] K. Kaneko, H. Kawanowa, H. Ito, and S. Fujita, Evaluation of misfit relaxation in α-Ga_2O_3 epitaxial growth on α-Al_2O_3, Japanese Journal of Applied Physics **51**, 3 (2012).

[19] R. Jinno, K. Kaneko, and S. Fujita, Thermal stability of α-Ga_2O_3 films grown on c-plane sapphire substrates via mist-CVD, AIP Advances **10**, 115013 (2020).

[20] K. Akaiwa, K. Kaneko, K. Ichino, and S. Fujita, Conductivity control of Sn-doped α-Ga_2O_3 thin films grown on sapphire substrates, Japanese Journal of Applied Physics **55**, 1202BA (2016).

[21] K. Akaiwa, K. Ota, T. Sekiyama, T. Abe, T. Shinohe, and K. Ichino, Electrical Properties of Sn-Doped α-Ga_2O_3 Films on m-Plane Sapphire Substrates Grown by Mist Chemical Vapor Deposition, physica status solidi (a) **217**, 1900632 (2020).

[22] G. T. Dang, S. Sato, Y. Tagashira, T. Yasuoka, L. Liu, and T. Kawaharamura, α-$(Al_xGa_{1-x})_2O_3$ single-layer and heterostructure buffers for the growth of conductive Sn-doped α-Ga_2O_3 thin films via mist chemical vapor deposition, APL Materials **8**, 101101 (2020).

[23] R. Jinno, T. Uchida, K. Kaneko, and S. Fujita, Reduction in edge dislocation density in corundum-structured α-Ga_2O_3 layers on sapphire substrates with quasi-graded α-(Al,Ga)$_2$O$_3$ buffer layers, Applied Physics Express **9**, 071101 (2016).

[24] H. M. Ng, D. Doppalapudi, T. D. Moustakas, N. G. Weimann, and L. F. Eastman, The role of dislocation scattering in n -type GaN films, Applied Physics Letters **73**, 821 (1998).

[25] H. Son, Y. ji Choi, J. hyeon Park, B. Ryu, and D. woo Jeon, Correlation of Pulsed Gas Flow on Si-doped α-Ga_2O_3 Epilayer Grown by Halide Vapor Phase Epitaxy, ECS Journal of Solid State Science and Technology **9**, 055005 (2020).

[26] T. Harwig, G. Wubs, and G. Dirksen, Electrical Properties of β-Ga_2O_3 Single Crystals, Solid State Communications **18**, 1223 (1976).

[27] T. Harwig and J. Schoonman, Electrical properties of β-Ga_2O_3 single crystals. II, Journal of Solid State Chemistry **23**, 205 (1978).

[28] M. Saleh, A. Bhattacharyya, J. B. Varley, S. Swain, J. Jesenovec, S. Krishnamoorthy, and K. Lynn, Electrical and optical properties of Zr doped β-Ga_2O_3 single crystals, Applied Physics Express **12**, 3 (2019).

[29] D. Wickramaratne, J. B. Varley, and J. L. Lyons, Donor doping of corundum $(Al_xGa_{1-x})_2O_3$, Applied Physics Letters **121**, 1 (2022).

[30] F. Massabuau, D. Nicol, F. Adams, J. Jarman, J. Roberts, A. Kovács, P. Chalker, and R. Oliver, Study of Ti contacts to corundum α-Ga_2O_3, Journal of Physics D: Applied Physics **54**, 384001 (2021).

[31] H. von Wenckstern, M. Brandt, G. Zimmermann, J. Lenzner, M. Lorenz, and M. Grundmann, Temperature Dependent Hall Measurements on PLD Thin Films, MRS Online Proceedings Library **957** (2006).

[32] L. J. van der Pauw, A method of measuring the resistivity and Hall coefficient on lamellae of arbitrary shape, Philips Technical Review **20**, 220 (1958).

[33] L. J. van der Pauw, A method of Measuring Specific Resistivity and Hall Effect of Discs of Arbitrary Shape, Philips Research Reports **13**, 1 (1958).

[34] S. Köpp, C. Petersen, D. Splith, M. Grundmann, and H. von Wenckstern, Properties of Schottky barrier diodes on heteroepitaxial α-Ga_2O_3 thin films, Journal of Vacuum Science & Technology A **41**, 1 (2023).

[35] M. Kneiß, D. Splith, H. von Wenckstern, M. Lorenz, T. Schultz, N. Koch, and M. Grundmann, Strain states and relaxation for α-$(Al_xGa_{1-x})_2O_3$ thin films on prismatic planes of α-Al_2O_3 in the full composition range: Fundamental difference of a- and m-epitaxial planes in the manifestation of shear strain and lattice tilt, Journal of Materials Research **36**, 4816 (2021).

[36] J. C. Slater, Atomic Radii in Crystals, The Journal of Chemical Physics **41**, 3199 (1964).

[37] R. D. Shannon, Revised Effective Ionic Radii and Systematic Studies of Interatomie Distances in Halides and Chaleogenides (1976).

[38] T. Uchida, K. Kaneko, and S. Fujita, Electrical characterization of Si-doped n-type α-Ga_2O_3 on sapphire substrates, MRS Advances **3**, 171 (2018).

[39] B. K. Ridley, Reconciliation of the Conwell-Weisskopf and Brooks-Herring formulae for charged-impurity scattering in semiconductors: Third-body interference, Journal of Physics C: Solid State Physics **10**, 1589 (1977).

[40] D. Chattopadhyay and H. J. Queisser, Electron scattering by ionized impurities in semiconductors, Reviews of Modern Physics **53**, 745 (1981).

[41] W. Read, LXXXVII. Theory of dislocations in germanium, The London, Edinburgh, and Dublin Philosophical Magazine and Journal of Science **45**, 775 (1954).

[42] B. Pödör, Electron Mobility in Plastically Deformed Germanium, physica status solidi (b) **16**, 4 (1966).

[43] .

[44] D. Splith, S. Müller, H. von Wenckstern, and M. Grundmann, Numerical Modeling of Schottky Barrier Diode Characteristics, Physica Status Solidi (A) Applications and Materials Science **218**, 2100121 (2021).

[45] D. Splith, S. Müller, F. Schmidt, H. V. Wenckstern, J. J. V. Rensburg, W. E. Meyer, and M. Grundmann, Determination of the mean and the homogeneous barrier height of Cu Schottky contacts on heteroepitaxial β-Ga_2O_3 thin films grown by pulsed laser deposition, Physica Status Solidi (A) Applications and Materials Science **211**, 40 (2014).

[46] S. Müller, H. V. Wenckstern, F. Schmidt, D. Splith, H. Frenzel, and M. Grundmann, Method of choice for the fabrication of high-quality β-gallium oxide-based Schottky diodes, Semiconductor Science and Technology **32**, 65013 (2017).

[47] E. Chikoidze, H. J. V. Bardeleben, K. Akaiwa, E. Shigematsu, K. Kaneko, S. Fujita, and Y. Dumont, Electrical, optical, and magnetic properties of Sn doped α-Ga_2O_3 thin films, Journal of Applied Physics **120**, 025109 (2016).

[48] G. T. Dang, Y. Tagashira, T. Yasuoka, L. Liu, and T. Kawaharamura, Conductive Si-doped α-$(Al_xGa_{1-x})_2O_3$ thin films with the bandgaps up to 6.22 eV, AIP Advances **10**, 115019 (2020).

[49] G. T. Dang, T. Kawaharamura, M. Furuta, and M. W. Allen, Mist-CVD Grown Sn-Doped α-Ga_2O_3 MESFETs, IEEE Transactions on Electron Devices **62**, 3640 (2015).

[50] A. J. Green, J. Speck, G. Xing, P. Moens, F. Allerstam, K. Gumaelius, T. Neyer, A. Arias-Purdue, V. Mehrotra, A. Kuramata, K. Sasaki, S. Watanabe, K. Koshi, J. Blevins, O. Bierwagen, S. Krishnamoorthy, K. Leedy, A. R. Arehart, A. T. Neal, S. Mou, S. A. Ringel, A. Kumar, A. Sharma, K. Ghosh, U. Singisetti, W. Li, K. Chabak, K. Liddy, A. Islam, S. Rajan, S. Graham, S. Choi, Z. Cheng, and M. Higashiwaki, β-Gallium oxide power electronics, APL Materials **10**, 029201 (2022).

[51] M. Grundmann and M. Lorenz, Azimuthal Anisotropy of Rhombohedral (Corundum Phase) Heterostructures, physica status solidi (b) **2100104**, 2100104 (2021).

[52] M. Grundmann, T. Stralka, M. Lorenz, S. Selle, C. Patzig, and T. Höche, Plastic strain relaxation and alloy instability in epitaxial corundum-phase $(Al,Ga)_2O_3$ thin films on r-plane Al_2O_3, Materials Advances **2**, 4316 (2021).

[53] M. Grundmann, T. Stralka, and M. Lorenz, Epitaxial growth and strain relaxation of corundum-phase $(Al,Ga)_2O_3$ thin films from pulsed laser deposition at 1000°C on r-plane Al_2O_3, Applied Physics Letters **117**, 242102 (2020).

[54] A. Hassa, H. von Wenckstern, L. Vines, and M. Grundmann, Influence of Oxygen Pressure on Growth of Si-Doped β-$(Al_x Ga_{1-x})_2O_3$ Thin Films on c-Sapphire Substrates by Pulsed Laser Deposition, ECS Journal of Solid State Science and Technology **8**, Q3217 (2019).

[55] M. Higashiwaki, K. Sasaki, A. Kuramata, T. Masui, and S. Yamakoshi, Gallium oxide (Ga_2O_3) metal-semiconductor field-effect transistors on single-crystal β-Ga_2O_3 (010) substrates, Applied Physics Letters **100**, 013504 (2012).

[56] Y. J. Jeong, J. H. Park, M. J. Yeom, I. Kang, J. Y. Yang, H. Y. Kim, D. W. Jeon, and G. Yoo, Heteroepitaxial α-Ga_2O_3 MOSFETs with a 2.3 kV breakdown voltage grown by halide vapor-phase epitaxy, Applied Physics Express **15**, 074001 (2022).

[57] R. Jinno, N. Yoshimura, K. Kaneko, and S. Fujita, Enhancement of epitaxial lateral overgrowth in the mist chemical vapor deposition of α-Ga_2O_3 by using a-plane sapphire substrate, Japanese Journal of Applied Physics **58**, 120912 (2019).

[58] R. Jinno, T. Uchida, K. Kaneko, and S. Fujita, Control of Crystal Structure of Ga_2O_3 on Sapphire Substrate by Introduction of α-$(Al_xGa_{1-x})_2O_3$ Buffer Layer, physica status solidi (b) **255**, 1700326 (2018).

[59] C. Joishi, S. Rafique, Z. Xia, L. Han, S. Krishnamoorthy, Y. Zhang, S. Lodha, H. Zhao, and S. Rajan, Low-pressure CVD-grown β-Ga_2O_3 bevel-field-plated Schottky barrier diodes, Applied Physics Express **11**, 031101 (2018).

[60] S.-I. Kan, S. Takemoto, K. Kaneko, I. Takahashi, M. Sugimoto, T. Shinohe, and S. Fujita, Electrical properties of α-Ir_2O_3/α-Ga_2O_3 pn heterojunction diode and band alignment of the heterostructure, Applied Physics Letters **113**, 212104 (2018).

[61] K. Kaneko, Y. Masuda, S. I. Kan, I. Takahashi, Y. Kato, T. Shinohe, and S. Fujita, Ultra-wide bandgap corundum-structured p-type α-$(Ir,Ga)_2O_3$alloys for α-Ga_2O_3 electronics, Applied Physics Letters **118**, 102104 (2021).

[62] K. Kaneko, S. Fujita, T. Shinohe, and K. Tanaka, Progress in α-Ga_2O_3 for practical device applications (2023).

[63] K. Kawara, Y. Oshima, M. Okigawa, and T. Shinohe, Elimination of threading dislocations in α-Ga_2O_3 by double-layered epitaxial lateral overgrowth, Applied Physics Express **13**, 075507 (2020).

[64] M. Kneiß, A. Hassa, D. Splith, C. Sturm, H. von Wenckstern, T. Schultz, N. Koch, M. Lorenz, and M. Grundmann, Tin-assisted heteroepitaxial PLD-growth of κ-Ga_2O_3 thin films with high crystalline quality, APL Materials **7**, 022516 (2019).

[65] M. H. Lee and R. L. Peterson, Process and characterization of ohmic contacts for beta-phase gallium oxide, Journal of Materials Research **36**, 4771 (2021).

[66] M. H. Lee and R. L. Peterson, Interfacial reactions of titanium/gold ohmic contacts with Sn-doped β-Ga_2O_3, APL Materials **7**, 022524 (2019).

[67] M. Oda, R. Tokuda, H. Kambara, T. Tanikawa, T. Sasaki, and T. Hitora, Schottky barrier diodes of corundum-structured gallium oxide showing on-resistance of $0.1\mathrm{m\Omega cm^2}$ grown by mist epitaxy, Applied Physics Express **9**, 021101 (2016).

[68] M. Oda, K. Kaneko, S. Fujita, and T. Hitora, Crack-free thick (5 μm) α-Ga_2O_3 Thin Films on Sapphire Substrates with α-$(Al,Ga)_2O_3$ buffer layers, Japanese Journal of Applied Physics **55**, 1202b4 (2016).

[69] M. Oda, A. Takatsuka, T. Hitora, J. Kikawa, K. Kaneko, and S. Fujita, α-Ga_2O_3 Schottky barrier diodes fabricated by Mist Epitaxy technique.

[70] Y. Oshima, K. Kawara, T. Oshima, M. Okigawa, and T. Shinohe, Rapid growth of α-Ga_2O_3 by HCl-boosted halide vapor phase epitaxy and effect of precursor supply conditions on crystal properties, Semiconductor Science and Technology **35**, 055022 (2020).

[71] A. Segura, L. Artús, R. Cusc{o}, R. Goldhahn, and M. Feneberg, Band gap of corundumlike α-Ga_2O_3 determined by absorption and ellipsometry, Physical Review Materials **1**, 024604 (2017).

[72] P. Vogt and O. Bierwagen, Reaction kinetics and growth window for plasma-assisted molecular beam epitaxy of Ga_2O_3: Incorporation of Ga vs. Ga_2O desorption, Applied Physics Letters **108**, 072101 (2016).

[73] A. Zachinskis, J. Grechenkov, E. Butanovs, A. Platonenko, S. Piskunov, A. I. Popov, J. Purans, and D. Bocharov, Ir impurities in α- and β-Ga_2O_3 and their detrimental effect on p-type conductivity, Scientific Reports **13**, 1 (2023).